International Journal of Scientific Research and Engineering Development-– Volume 9 Issue 5, Sep-Oct 2026
Available at www.ijsred.com

RESEARCH ARTICLE OPEN ACCESS

Solar Energy System Design for a Net-Zero Energy Buildings Technology

Mohamed Hamza, Samar Alyagooubi
Mechanical Engg. Department, Gharian University, Gharian, Libya
hmzamohamed71@gmail.com and samaralamin1975@gmail.com

----------**********----------

Abstract

This paper combines a review of solar energy technologies, the physics of solar radiation and Sun–Earth geometry, and the design of a solar energy system intended to bring an elementary school in Gharyan, Libya, to net-zero energy operation, and it compares the site with Dayton, Ohio, where an earlier school design that is the main precedent for the Gharyan system was developed. The design couples 181 evacuated-tube collectors and a lithium bromide–water absorption chiller, sized with the f-chart, utilizability and phi-f chart methods for an annual solar fraction of 56%, with a 228 kW grid-connected photovoltaic (PV) array of 578 monocrystalline modules sized with PVWatts. The governing radiation equations are applied to both latitudes, and a monthly tilted-surface model, which reproduces NREL tilt data for Dayton within 2.1%, is used to compare the sites. Gharyan receives 48% more global horizontal irradiation than Dayton (2129 against 1438 kWh/m^2 per year), has one third of its heating degree-days and 2.5 times its cooling degree-days, and the same array would yield about 1630 kWh/kWp against 1140 kWh/kWp. The design methods transfer from Dayton to Gharyan, but the collector numbers, solar fractions and PV output do not: about 135 kW of PV would meet the Gharyan load, and the electricity tariff, under 1 US cent/kWh in Libya against 11.3 cents in Ohio, explains why a payback of about five years in Ohio cannot be expected in Libya.

***Index Terms*—absorption cooling, f-chart method, net-zero energy building, photovoltaics, solar geometry, solar radiation, tilted-surface irradiation.**

----------**********----------

I. Introduction

Energy supports almost every activity of modern life, from household devices to industrial plants and public infrastructure. World demand for oil, coal and natural gas keeps rising, the resources are finite, their cost is rising, and burning them releases the greenhouse gases that drive climate change [1]. Solar energy is one of the most promising answers because sunlight is free, abundant and available almost everywhere, especially in regions with high radiation through the year. Libya is one of those regions.

The problem that motivates this work is practical. Libyan schools suffer from frequent power outages that interrupt lessons, high electricity bills caused by the growing use of electronic devices, voltage instability that can damage sensitive equipment, and complete dependence on the national grid with no backup [1]. The working hypothesis is that a solar energy system will lower annual energy costs, make the supply more stable, reduce dependence on the grid, and raise environmental awareness among students.

Net-zero energy buildings (NZEBs) combine energy efficiency with renewable generation so that they produce as much energy as they consume over a year. Sartori *et al.* point out that the balance has no single meaning until the designer specifies what is balanced, over what period, and with what weighting of imported and exported energy [2], and Marszal *et al.* reach a similar conclusion after reviewing existing definitions and calculation methods [3]. In this paper the balance is an annual one on site energy: the building exports surplus electricity in sunny months and imports it in winter, and the two should cancel over the year.

The work was first reported as a review of solar technologies and prior research, an account of the radiation physics and geometry on which the design rests, and the design itself [1]. This paper includes a comparison with Dayton, Ohio, the site of an earlier school design that combines photovoltaic (PV) and thermal collectors and is the main precedent for the Gharyan system [1]. The comparison asks which parts of a net-zero school design transfer between the two climates and which must be recomputed.

II. Solar Energy Technologies and Prior Research

A. Solar Resource and Classification of Solar Systems

The solar energy reaching the Earth's surface each year is on the order of 5.5×10^{17} kWh, roughly a thousand times the projected human energy use of 4×10^{14} kWh per year and far larger than the wind resource base of 6×10^{14} kWh per year [1]. Resource size is therefore not the constraint; conversion, storage and cost are. Any renewable energy system is designed in three steps: characterize the resource, choose the conversion technology, and match it to the energy needs, whether electric power, heating or cooling. For solar systems the resource is described by radiation data at the level of detail the design needs (hourly, average daily, or the average day of the month), and the collector is chosen according to the application and the temperature required [1]. The resource figures are collected in Table I.

 ©IJSRED: All Rights are Reserved

TABLE I
ANNUAL ENERGY RESOURCE BASE AND HUMAN ENERGY USE [1]

Quantity	Energy (kWh/year)
Solar energy resource base	1.5×10^{18}
Solar resource on the Earth's surface	5.5×10^{17}
Wind energy resource base	6×10^{14}
Human energy use (mid- to late-century)	4×10^{14}

Solar applications fall into two groups (Fig. 1). Direct thermal uses convert radiation to heat: domestic hot water, swimming pool heating, active and passive space heating, solar cookers and solar cooling. Electricity is generated either thermally, through solar ponds, concentrating collectors and power towers, or directly by photovoltaics [1].

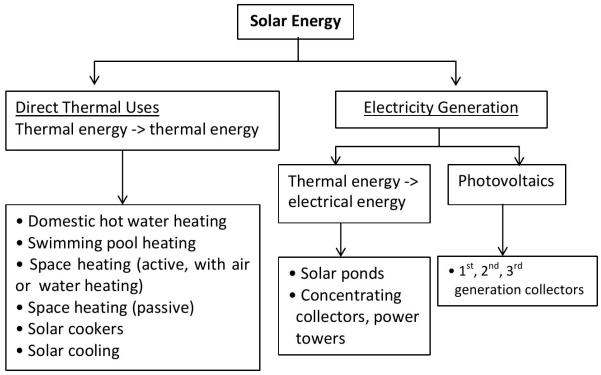

Fig. 1. Classification of solar energy systems according to use [1].

B. Photovoltaic Conversion and Efficiency Limits

A solar cell is a large-area p–n junction diode. Absorbed photons release electrons, and the junction separates the charges so that a current flows through an external circuit [1]. The cell is described by the ideal diode equation with a light-generated current [4], [5]:

$$I = I_L - I_0\left[\exp\left(\frac{qV}{nkT}\right) - 1\right] \tag{1}$$

where I_L is the light-generated current, I_0 the dark saturation current, q the electron charge, V the voltage, n the ideality factor, k Boltzmann's constant and T the absolute temperature. Setting $V = 0$ gives the short-circuit current $I_{sc} \approx I_L$, and setting $I = 0$ gives the open-circuit voltage

$$V_{oc} = \frac{nkT}{q}\ln\left(\frac{I_L}{I_0} + 1\right) \tag{2}$$

The fill factor and the conversion efficiency, the parameters used throughout the reviewed studies, are

$$FF = \frac{V_{mp}\, I_{mp}}{V_{oc}\, I_{sc}} \tag{3}$$

$$\eta = \frac{V_{oc}\, I_{sc}\, FF}{P_{in}} \tag{4}$$

where V_{mp} and I_{mp} are the voltage and current at the maximum power point and P_{in} is the incident solar power. Reducing recombination lowers I_0 and raises V_{oc}, and better light absorption raises I_{sc}.

The first silicon cell, announced by Chapin, Fuller and Pearson of Bell Laboratories in 1954, reached about 6% [6]. Zhao *et al.* later reported 24.4% for a monocrystalline and 19.8% for a multicrystalline cell with a honeycomb texture that reduces reflection and traps light [7]. Inverted pyramids, dielectric reflectors and doping that reduces recombination losses account for this fourfold gain [5]. A photon is converted only if its energy exceeds the band gap E_g, so the longest usable wavelength, in µm for E_g in eV, is

$$\lambda_g = \frac{1.24}{E_g} \tag{5}$$

which is about 1.1 µm for silicon. Shockley and Queisser showed from the principle of detailed balance that a single-junction cell losing energy only through radiative recombination cannot exceed about 30%, with the best band gap near 1.1 eV [8]. Silicon's band gap is close to that value, which helps explain why silicon dominates the industry, and tandem and multi-junction cells, which stack junctions tuned to different parts of the spectrum, are reported to exceed 30% [1]. Gallium arsenide reaches a higher open-circuit voltage than silicon but a lower short-circuit current because of its larger band gap [1].

C. Generations of Photovoltaic Technology

PV technology is usually organized in generations (Table II). The first generation, crystalline silicon, dominates the market because it is stable and efficient; the second, thin film, uses less material; the third aims at higher efficiency and flexibility [1]. Pastuszak and Węgierek add a fourth, graphene-based generation and conclude that improving silicon remains relevant because silicon dominates the market [9]. Dye-sensitized cells, in which a dye on mesoporous titanium dioxide absorbs light and injects electrons, exceed 11% efficiency and can be made transparent or colored for building integration [10], but they are less efficient than silicon. For a school roof, where area is available and reliability matters most, ordinary crystalline silicon is the better choice.

TABLE II
GENERATIONS OF PHOTOVOLTAIC CELLS [1], [9]

Generation	Technologies	Main features
First	Monocrystalline and polycrystalline silicon	Stable and efficient; dominates the market
Second	Thin film: CdTe, CIGS	Lower production cost and material use
Third	Perovskite, dye-sensitized, quantum-dot, tandem	Higher efficiency potential and flexibility
Fourth	Graphene-based concepts	Under research

D. Solar Thermal Technologies

The thermal technologies are summarized in Table III. Solar water heaters use glazed, unglazed or evacuated-tube collectors with tank or pool storage. Passive solar heating admits the low winter Sun through equator-facing windows, stores the heat in the building structure and shades the high summer Sun; it can supply 20–50% of the heating-season demand and adds little or no cost to new buildings (Fig. 2) [1]. In a solar pond, dense salt water at the bottom reaches about 90°C beneath lighter fresh water at about 30°C, and the difference drives a vapor-cycle turbine. Parabolic troughs heat a synthetic oil to about 400°C;

 ©IJSRED: All Rights are Reserved

Luz International brought nine plants of 13–80 MW on line in the Mojave Desert by 1990. In a power tower a heliostat field concentrates sunlight on a central receiver; the 10 MW plant at Barstow, California, operated from the early 1980s, and later designs with molten-salt storage run around the clock [1]. Flat-plate and evacuated-tube collectors can also drive lithium bromide (LiBr)–water absorption chillers, which reduce electricity use in summer [1]. This matters in Libya, where the largest loads fall in the hottest months.

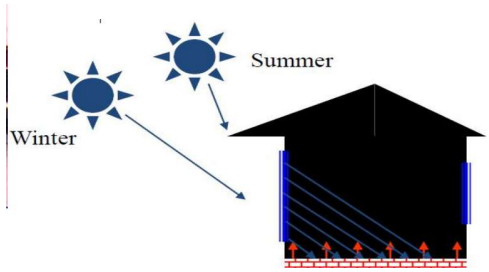

Fig. 2. Principle of passive solar heating: the low winter Sun is admitted and the high summer Sun is shaded [1].

TABLE III
SUMMARY OF SOLAR THERMAL TECHNOLOGIES [1]

Technology	Collector or medium	Typical figures	Use
Water heating	Glazed, unglazed, evacuated tube	Tank or pool storage	Hot water
Passive heating	Equator-facing windows, thermal mass	20–50% of space heating	Space heating
Solar pond	Salt-gradient pond	About 90°C at the bottom	Electricity
Parabolic trough	Line focus, synthetic oil	About 400°C; 13–80 MW	Electricity
Power tower	Heliostat field, molten salt	Hundreds of °C; 10 MW	Electricity
Solar cooling	Collectors with LiBr–water chiller	Heat-driven cycle	Cooling

E. Energy Storage

Sunlight is intermittent, and storage is one of the main challenges of solar power. Lithium-ion batteries offer high energy density and efficiency, while thermal storage suits long retention [1]. Zakeri and Syri compiled life-cycle costs for pumped hydro, compressed air, flywheels, batteries, flow batteries, supercapacitors and hydrogen and found that no technology is cheapest for every grid service [11]. Batteries have a limited number of cycles and respond slowly, while supercapacitors exchange energy rapidly at high power; Jing *et al.* reviewed battery–supercapacitor hybrids in standalone microgrids, in which the supercapacitor absorbs fast fluctuations so that the battery lasts longer [12]. Wang *et al.* placed a molecular solar thermal layer in front of a silicon cell; the layer stores the energy of high-energy photons in chemical bonds, lowers the cell temperature by about 8°C, and gives a chemical storage efficiency of up to 2.3% and a total solar utilization efficiency of 14.9% [13].

F. Environmental and Economic Evidence

Life-cycle assessments report energy payback times of about 0.75–3.5 years for thin-film and 1.7–2.7 years for monocrystalline silicon systems, with CdTe performing best [14], so a module returns the energy used to make it many times over its life. Large installations affect land, soil, water, biodiversity and health, but these effects are low compared with other energy systems when sites and designs are chosen carefully [15]; a rooftop system on an existing school avoids most land-use concerns. The initial investment is relatively high, but savings on energy bills and maintenance make solar advantageous over time, and subsidies and tax incentives improve the return [1]. The global average cost of electricity from utility-scale PV fell 89% between 2010 and 2025, to 0.044 US$/kWh [16]. Kannan and Vakeesan find that solar compares well with other renewable sources in availability, cost, accessibility, capacity and efficiency [17], while Kabir *et al.* list the barriers that remain: cell efficiency, upfront cost, financing, infrastructure and skills [18].

G. Operating Challenges and Smart Monitoring

The practical difficulties of solar power are efficiency losses at high temperature, dust on the panels, and the area required [1]. Mani and Pillai reviewed how dust deposition degrades PV output, what governs its settling, and how it can be mitigated [19]; in a dry climate such as Gharyan's a cleaning schedule belongs in the design. Artificial intelligence, the Internet of Things and smart grids allow generation forecasting, orientation optimization and real-time fault detection [1], and Mellit and Kalogirou concluded that neural networks, fuzzy logic and genetic algorithms are promising tools for forecasting, sizing, modeling and control of PV systems [20].

H. Summary of the Reviewed Studies

The sixteen studies reviewed in [1] are summarized in Table IV. Early work concentrated on the physics of conversion and on cell efficiency, while later work turned to hybrid systems, storage and building integration. The body of work has limits. Few studies concern North Africa, where heat, dust and a subsidized electricity price change both the engineering and the economics, and storage, monitoring and building integration are treated as separate topics, although a school system must solve them together. Study 10, the Dayton school, is the closest precedent for the present design and the basis of the comparison in Section VII.

 ©IJSRED: All Rights are Reserved

TABLE IV
SUMMARY OF THE SIXTEEN REVIEWED STUDIES [1]

No.	Subject	Main finding
1	PV conversion	Si cell efficiency rose from about 6% (1954) to more than 24%
2	Solar electricity	Falling module cost and rising efficiency make grid and off-grid PV viable
3	Sustainable development	PV, solar thermal and CSP cut emissions; sunny developing countries gain most
4	Supercapacitor storage	Fast storage and high power density improve PV reliability
5	Hybrid PV–MOST device	Electricity plus chemical heat storage raises solar utilization
6	PV generations	Crystalline Si; thin film; perovskite, dye and quantum-dot cells
7	Dye-sensitized cells	Cheap and suited to building integration, but less efficient
8	Generation challenges	Heat, dust and land limit output; cooling, storage and AI help
9	PV energy conversion	Texturing, antireflection coatings and tandem cells raise absorption
10	Solar systems in NZEBs	Dayton, Ohio school: f > 56%, 578 PV and 181 thermal collectors, payback ≈5 years
11	Solar heating and cooling	Collectors with LiBr–water absorption reduce summer electricity use
12	Storage for solar	Li-ion for density, thermal storage for long retention, hybrids for flexibility
13	Environmental impact	Life-cycle footprint far below fossil fuels; recycling matters
14	Efficiency innovations	Light trapping, multi-junction, perovskite and quantum-dot cells beyond 30%
15	Economic assessment	High first cost offset by savings; incentives improve the return
16	Future integration	AI, IoT and smart grids enable prediction and fault detection

III. SOLAR RADIATION AND SUN–EARTH GEOMETRY

The output of any solar system depends first on how much sunlight reaches the collector, and that quantity is set by physics and geometry before any equipment is chosen. Four characteristics decide how sunlight interacts with a collector: its spectral content, the power density from the Sun, the angle at which the radiation strikes the collector, and the energy received over a day or a year [1]. The treatment follows Honsberg and Bowden [4] and Duffie and Beckman [21], and the results are evaluated for both sites.

A. Photons and the Solar Spectrum

Sunlight is electromagnetic radiation, and the band between 0.1 and 100 µm is called thermal radiation because it is both caused by and affects the temperature of matter [1]. A photon of wavelength λ carries the energy

$$E = \frac{hc}{\lambda} \tag{6}$$

where $h = 6.626\times10^{-34}$ J·s is Planck's constant and $c = 2.998\times10^{8}$ m/s the speed of light. With E in eV (1 eV = 1.602×10^{-19} J) and λ in µm, (6) becomes $E = 1.24/\lambda$, the relation used in (5); a green photon at 0.55 µm carries about 2.25 eV. The photon flux Φ, the number of photons striking a unit area per second, sets the current of a cell, and the power density in W/m² is

$$G = \Phi \frac{hc}{\lambda} \tag{7}$$

Real sources contain many wavelengths and are described by their spectral irradiance, the power density per unit wavelength in $W\cdot m^{-2}\cdot\mu m^{-1}$; lamps are imperfect substitutes for sunlight in testing because their spectra differ from the Sun's [4]. The Sun's spectrum is close to that of a blackbody, whose total power density and peak wavelength follow the Stefan–Boltzmann and Wien laws:

$$G = \sigma T^4 \tag{8}$$

$$\lambda_{peak} = \frac{2900}{T} \tag{9}$$

where $\sigma = 5.67\times10^{-8}$ $W\cdot m^{-2}\cdot K^{-4}$, T is in kelvin and λ_{peak} in µm. Nuclear fusion in the core converts hydrogen to helium, and the visible surface, the photosphere, is at about 6000 K [1]. Applying (8) and (9) at 6000 K gives a surface power density of about 7.3×10^{7} W/m² and a peak near 0.48 µm, inside the visible band where the eye is most sensitive (Fig. 3).

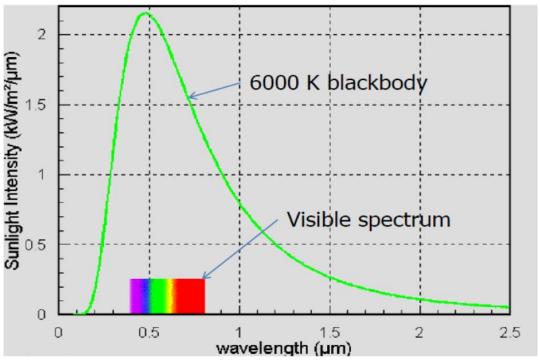

Fig. 3. Spectrum of a 6000 K blackbody compared with the visible range [1].

B. Radiation Outside the Atmosphere

The power density falls with the square of the distance from the Sun. At a distance D it is

$$G_0 = \frac{R_{sun}^2}{D^2} G_{sun} \tag{10}$$

where G_{sun} is the power density at the Sun's surface from (8) and R_{sun} the radius of the Sun. At the mean Earth–Sun distance this gives the solar constant G_{sc}, taken in [1] as 1.353 kW/m². That value is an older standard: Duffie and Beckman adopt 1367 W/m² [21], and satellite measurements put the total solar irradiance at 1360.8 ± 0.5 W/m² at solar minimum [22], so the value in [1] is about 0.6% low, a difference small beside the uncertainties of weather. Because the Earth's orbit is elliptical, the irradiance just outside the atmosphere varies through the year as

$$\frac{G}{G_{sc}} = 1 + 0.033\cos\left[\frac{360\,(n-2)}{365}\right] \tag{11}$$

where n is the day of the year. The irradiance is largest in January, when the Earth is closest to the Sun, which confirms that the seasons are caused by the tilt of the Earth's axis and not by its distance from the Sun.

 ©IJSRED: All Rights are Reserved

C. The Atmosphere and Air Mass

The atmosphere reduces the power through absorption, scattering and reflection, changes the spectral content, and introduces a diffuse component; water vapor, clouds and pollution have further local effects. In a typical clear sky about 70% of the radiation entering the atmosphere arrives directly, 7% reaches the ground as scattered light, 18% is absorbed and 3% is scattered back to space [1]. Beam radiation casts shadows and is the only part concentrating collectors can use, whereas flat PV modules use both beam and diffuse radiation. The air mass AM is the path length of light through the atmosphere normalized to the vertical path (Fig. 4). For a zenith angle Z,

$$AM = \frac{1}{\cos Z} \tag{12}$$

so that $AM = 1$ with the Sun overhead and $AM = 2$ at $Z = 60°$. Equation (12) treats the atmosphere as a flat layer and becomes infinite at sunrise; Kasten and Young give a form that allows for the curvature of the atmosphere [23]:

$$AM = \frac{1}{\cos Z + 0.50572\,(96.07995 - Z)^{-1.6364}} \tag{13}$$

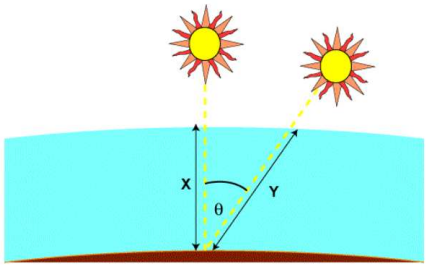

Fig. 4. Air mass as the ratio of the path length Y to the vertical path X [1], [4].

The clear-sky intensity of the direct component on a plane normal to the rays, in kW/m^2, follows the empirical relation

$$I_D = 1.353 \times 0.7^{(AM^{0.678})} \tag{14}$$

in which 1.353 kW/m^2 is the solar constant, 0.7 represents the fraction of radiation transmitted, and the exponent 0.678 fits the non-uniformity of the atmospheric layers. Intensity increases with height h above sea level, in km, as [1]

$$I_D = 1.353\left[(1 - ah)\,0.7^{(AM^{0.678})} + ah\right] \tag{15}$$

with $a = 0.14$. Even on a clear day the diffuse radiation is about 10% of the direct component, so the global irradiance on a surface facing the Sun is $I_G = 1.1 I_D$. At AM 1.5, the condition used to rate PV modules, (14) gives 0.85 kW/m^2 and $I_G = 0.93$ kW/m^2, close to the 1 kW/m^2 of standard test conditions. The height correction (15) raises the intensity at AM 1.5 by about 4.6% at Gharyan (about 0.55 km, Section IV) and 2.6% at Dayton (0.31 km).

D. Locating the Sun

Solar calculations use solar time, in which noon is the moment the Sun crosses the local meridian. Solar time differs from clock time by a longitude correction and by the equation of time E_t, in minutes (Fig. 5) [1]:

$$\begin{aligned} E_t &= 9.87\sin 2B - 7.53\cos B - 1.5\sin B \\ B &= 360\,(n - 81)/365 \end{aligned} \tag{16}$$

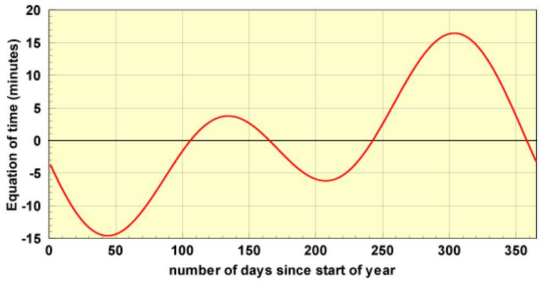

Fig. 5. The equation of time through the year [1], [4].

The declination δ, the angle between the Sun's rays and the plane of the equator, varies between ±23.45° because the Earth's axis is tilted, and is zero only at the equinoxes (Fig. 6):

$$\delta = 23.45° \sin\left[\frac{360\,(284 + n)}{365}\right] \tag{17}$$

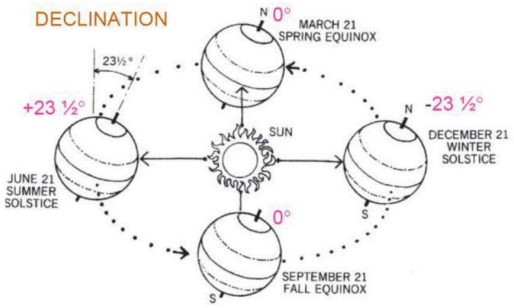

Fig. 6. Declination at the solstices and equinoxes [1].

The solar altitude β is the angle between the line to the Sun and the horizontal plane, and the solar azimuth φ is the angle between due south and the projection of that line, negative to the east and positive to the west. Both depend on the latitude L and on the hour angle $\omega = 15°(t_s - 12)$, where t_s is solar time in hours:

$$\sin\beta = \cos L\cos\delta\cos\omega + \sin L\sin\delta \tag{18}$$

$$\cos\phi = \frac{\sin\beta\sin L - \sin\delta}{\cos\beta\cos L} \tag{19}$$

For a surface tilted at Σ from the horizontal with surface azimuth ψ (Fig. 7), the surface–solar azimuth is $\gamma = \varphi - \psi$, and the angle of incidence θ between the surface normal and the rays follows from

$$\cos\theta = \cos\beta\cos\gamma\sin\Sigma + \sin\beta\cos\Sigma \tag{20}$$

 ©IJSRED: All Rights are Reserved

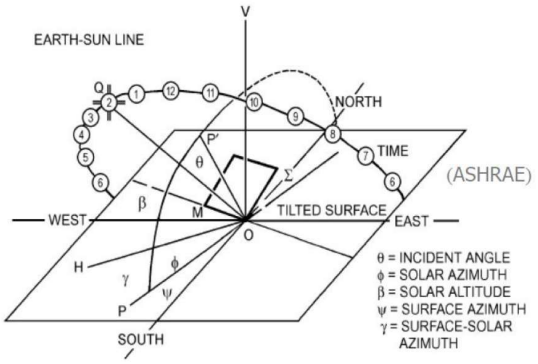

Fig. 7. Solar angles for a tilted surface [1]. Original figure: ASHRAE.

Beam radiation on the surface is proportional to cos θ, so a small angle of incidence is the aim of every orientation decision. At solar noon $\omega = 0$, $\varphi = 0$ and (18) reduces to $\beta = 90° - L + \delta$. A south-facing surface tilted at $\Sigma = L$ then receives the noon Sun at $\theta = |\delta|$, so the latitude tilt keeps the noon incidence angle below 23.45° in every season and the noon beam radiation at no less than about 92% of its value on a surface facing the Sun. This is the reason for the common rule that a fixed collector should be tilted at about the latitude angle.

E. Radiation Quantities, Clear-Sky Models and Shading

Total radiation on a surface is the sum of beam, diffuse and ground-reflected radiation; on a horizontal surface it is called global radiation. Irradiance G is the rate at which radiant energy is incident on a surface (W/m^2), and irradiation is the energy received over a period, with the symbols H for daily and I for hourly values [1]. Where measurements are unavailable, the ASHRAE clear-sky model gives the hourly beam radiation on a plane normal to the rays and the diffuse radiation on a horizontal surface as

$$I_b = A\,C_N \exp\left(-\frac{k}{\sin\beta}\right), \qquad I_d = C\,I_b \tag{21}$$

where A is the apparent extraterrestrial radiation, k the atmospheric extinction coefficient, C the diffuse sky factor and C_N the clearness number. A, k and C are tabulated for the 21st day of each month [1]. Clearness numbers are mapped for the United States but not for Libya, where a value near 1.0 has to be assumed. Sun-path diagrams show the path of the Sun across the sky at different times of year; in the northern hemisphere the noon Sun is highest on 21 June and lowest on 21 December and lies to the south (Fig. 8). The diagrams are used to design shading: an overhang that just shades a window of height h_w when the solar altitude is β (Fig. 9) has length

$$L_o = h_w \tan(90° - \beta) \tag{22}$$

Sized for the June noon Sun, such an overhang projects only $0.15h_w$ at Gharyan, where β = 81.3°, against $0.30h_w$ at Dayton, where β = 73.5°.

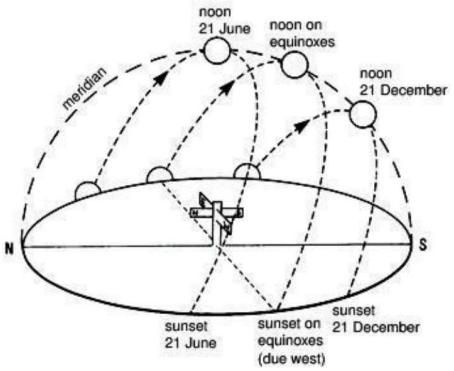

Fig. 8. Sun paths in the northern hemisphere [1].

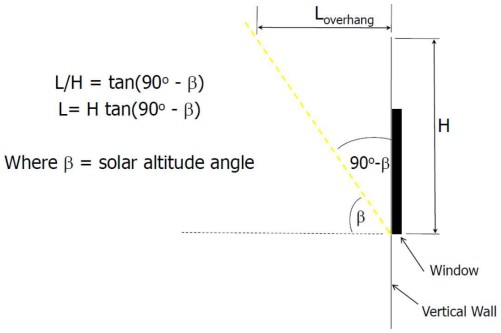

Fig. 9. Geometry of an overhang for shading design; H in the figure is the window height h_w [1].

IV. Sites, Data and Design Methods

A. Sites and Weather Data

The school is in Gharyan, at 32.17° N, 13.02° E; the mean pressure of 94.8 kPa in its weather data corresponds to an elevation of about 550 m. The design weather data were taken from RETScreen [1]. For Dayton the data are the 1961–1990 averages for the Dayton International Airport station (39.90° N, 84.22° W, 306 m) in the NREL solar radiation data manual [24]. Monthly temperature, global horizontal irradiation and degree-days for both sites are listed in Table V. The Gharyan data also give relative humidity of 48–66%, wind speeds of 3.5–4.7 m/s and pressures of 94.5–95.0 kPa [1], and the Dayton data relative humidity of 64–76% and wind speeds of 3.3–5.1 m/s [24]. Gharyan's daily radiation rises from 3.3 kWh/m^2 in December to 8.4 kWh/m^2 in July, in step with its cooling load, whereas Dayton's ranges from 1.5 to 6.2 kWh/m^2.

 ©IJSRED: All Rights are Reserved

TABLE V
MONTHLY CLIMATE DATA FOR GHARYAN (G) [1] AND DAYTON (D) [24]

Month	$\bar{T}_a$ (°C)		$\bar{H}$ (kWh/m²·d)		HDD (°C·d)		CDD (°C·d)	
	G	D	G	D	G	D	G	D
Jan	9.5	−3.3	3.4	1.9	260	672	0	0
Feb	10.8	−1.4	4.2	2.6	210	554	0	0
Mar	13.5	4.7	5.2	3.6	140	422	0	0
Apr	17.2	10.7	6.3	4.7	60	230	20	0
May	21.5	16.5	7.4	5.7	10	103	110	46
Jun	25.8	21.3	8.1	6.2	0	6	220	96
Jul	28.5	23.4	8.4	6.0	0	0	300	158
Aug	28.2	22.3	7.9	5.4	0	3	290	128
Sep	25.0	18.8	6.5	4.4	0	41	180	54
Oct	20.8	12.3	5.2	3.2	20	197	80	10
Nov	15.2	6.1	4.0	2.0	110	368	10	0
Dec	11.0	−0.2	3.3	1.5	220	575	0	0
Year	18.9	10.9	5.83	3.94	1030	3171	1210	492

Degree-days are referred to 18.3°C for Dayton and to about 18°C in the Gharyan data. Year: mean temperature and daily irradiation, total degree-days.

B. Design Approach

The aim of the design is an annual solar supply equal to the building demand. A solar combi-system delivers heat from the collectors for space heating and domestic hot water (DHW) in all seasons and, here, also drives an absorption chiller for cooling; auxiliary energy supplies the load when the solar supply falls short. A grid-connected PV system covers the electrical load, including the part of the thermal load that the collectors cannot meet [1]. A combi-system reduces operating cost and CO_2 emissions by saving primary energy and electricity.

C. The f-Chart Method

The f-chart method, derived by Klein, Beckman and Duffie from a large number of detailed simulations [25], is used to design active heating systems with storage and a minimum delivery temperature of about 20°C. The fraction f of the monthly load supplied by solar energy is a function of two dimensionless groups [1], [21]:

$$X = \frac{A_c F_R{}' U_L (T_{ref} - \bar{T}_a)\Delta t}{Q_L} \tag{23}$$

$$Y = \frac{A_c F_R{}' \overline{\tau\alpha}\, \bar{H}_T N}{Q_L} \tag{24}$$

where A_c is the collector area, F_R' the collector–heat exchanger efficiency factor, U_L the overall loss coefficient, $T_{ref} = 100$°C, $\bar{T}_a$ the monthly mean ambient temperature, Δt the number of seconds in the month, Q_L the monthly load, $(\tau\alpha)$ the monthly mean transmittance–absorptance product, $\bar{H}_T$ the monthly mean daily radiation on the collector and N the number of days in the month. X is the ratio of reference collector losses to the load and Y the ratio of absorbed solar energy to the load. For liquid systems with the standard storage of 75 L per m² of collector,

$$f = 1.029Y - 0.065X - 0.245Y^2 + 0.0018X^2 + 0.0215Y^3 \tag{25}$$

and other storage volumes M are handled by multiplying X by $(M/75)^{-0.25}$ for $37.5 \le M \le 300$ L/m² [21].

D. The Utilizability and Phi-f Chart Methods

Utilizability rests on the idea that there is a critical radiation level below which no useful energy is collected. The concept was developed by Whillier and by Hottel and Whillier and extended by Liu and Jordan and by Klein [1], [21]. It applies when the collector inlet temperature $\bar{T}_i$ is constant through the month, and gives the critical level and the monthly useful energy as

$$G_c = \frac{F_R U_L (\bar{T}_i - \bar{T}_a)}{F_R\, \overline{\tau\alpha}} \tag{26}$$

$$q_u = A_c F_R\, \overline{\tau\alpha}\, \bar{H}_T\, \bar{\phi} \tag{27}$$

where $\bar{\varphi}$ is the monthly mean daily utilizability, correlated with the clearness index, a geometric factor and the dimensionless critical level. The phi-f chart method of Klein and Beckman [26] combines the two approaches for closed-loop systems with tank storage whose delivery temperature is well above 20°C, as when solar heat drives an absorption chiller. The solar fraction is correlated with modified groups:

$$X' = \frac{A_c F_R U_L (F_R'/F_R) T_{ref}\, \Delta t}{Q_L} \tag{28}$$

$$Y' = \bar{\phi}_{max} \frac{A_c F_R (\tau\alpha)_n (F_R'/F_R)}{Q_L} \times \frac{\overline{\tau\alpha}}{(\tau\alpha)_n} \bar{H}_T N \tag{29}$$

where $(\tau\alpha)_n$ is the transmittance–absorptance product at normal incidence. For collectors tilted within ±15° of the latitude the ratio of the monthly mean to the normal-incidence product is 0.96 from October to March and 0.90 from April to September [1]. The heat exchanger correction is

$$\frac{F_R'}{F_R} = \left[1 + \frac{F_R U_L}{\dot{m} c_p}\left(\frac{1}{\varepsilon_c} - 1\right)\right]^{-1} \tag{30}$$

where $\dot{m}$ is the collector flow rate per unit area, c_p the fluid specific heat and ε_c the heat exchanger effectiveness, and the solar fraction follows from

$$f = Y' - 0.015[e^{3.85f} - 1] \times [1 - e^{-0.15X'}] R_s^{0.76} \tag{31}$$

where $R_s = R/350$ is the storage ratio and R the storage capacity per unit collector area (kJ·m^{-2}·°C^{-1}). Because f appears on both sides, (31) is solved by iteration.

E. Radiation on the Collector Plane

For each month the declination (17), the sunset hour angle and the daily extraterrestrial radiation on a horizontal surface are evaluated as [21]

$$\cos\omega_s = -\tan L \tan\delta \tag{32}$$

$$\bar{H}_o = \frac{24 \times 3600\, G_{sc}}{\pi}\left[1 + 0.033\cos\frac{360\, n}{365}\right] \times \left(\cos L\cos\delta\sin\omega_s + \frac{\pi\omega_s}{180}\sin L\sin\delta\right) \tag{33}$$

 ©IJSRED: All Rights are Reserved

and the monthly mean clearness index is $\bar{K}_T = \bar{H}/\bar{H}_o$. The diffuse fraction is estimated with the monthly correlation of Erbs *et al.* [27],

$$\frac{\bar{H}_d}{\bar{H}} = a_0 + a_1\bar{K}_T + a_2\bar{K}_T^2 + a_3\bar{K}_T^3 \tag{34}$$

with $(a_0,\ a_1,\ a_2,\ a_3) = (1.391,\ -3.560,\ 4.189,\ -2.137)$ for $\omega_s \le 81.4°$ and $(1.311,\ -3.022,\ 3.427,\ -1.821)$ otherwise, and the radiation on a south-facing surface tilted at Σ follows the isotropic-sky model

$$\bar{H}_T = \bar{H}\left(1 - \frac{\bar{H}_d}{\bar{H}}\right)\bar{R}_b + \bar{H}_d\frac{1+\cos\Sigma}{2} + \bar{H}\rho_g\frac{1-\cos\Sigma}{2} \tag{35}$$

where $\bar{R}_b$ is the ratio of monthly mean beam radiation on the tilted and horizontal surfaces [28] and $\rho_g = 0.2$ is the ground reflectance. The design spreadsheets of [1] use the same relations. Evaluated here with $G_{sc} = 1367$ W/m^2 and the recommended mean day of each month [21], the model reproduces the NREL latitude-tilt data for Dayton [24] within 2.1% over the year, with a mean monthly deviation of 4.0% (Fig. 10), and it is used for both sites in Section VII.

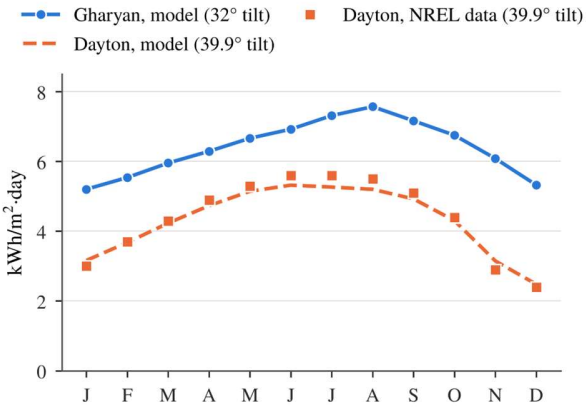

Fig. 10. Monthly mean daily irradiation on the latitude-tilted plane from (35), with the NREL tilt data for Dayton [24] used to validate the model.

F. Photovoltaic Output

In [1] the PV output was evaluated with PVWatts, which estimates hourly output from the location, the radiation incident on the array, the cell temperature, and the array size, type, tilt and losses [29]. For the site comparison a monthly estimate is used:

$$E_{AC} = P_{DC}\frac{\bar{H}_T N}{G_{STC}}[1 + \gamma_P(T_c - 25)]DF \tag{36}$$

where P_{DC} is the DC rating, $G_{STC} = 1$ kW/m^2, $\gamma_P = -0.0047$/°C is the power temperature coefficient of a standard PVWatts module [29], and $DF = 0.77$ is the DC-to-AC derate factor used in [1]. The cell temperature is estimated from the nominal operating cell temperature (NOCT) relation [21]

$$T_c = \bar{T}_a + (NOCT - 20)\frac{G_T}{800} \tag{37}$$

with $NOCT = 45$°C and a representative operating irradiance $G_T = 800$ W/m^2.

V. Solar Thermal System Design

A. Lithium Bromide–Water Absorption Chiller

In the absorption cycle (Fig. 11), heat from the solar collectors enters the generator and boils water out of the LiBr solution. The vapor condenses in the condenser and flows to the evaporator, where, at low pressure, it boils at a very low temperature and chills the water circuit. The strong solution in the absorber takes up the vapor and becomes a weak solution, which is pumped back to the generator [1]. The design conditions of the chiller-heater are listed in Table VI. From the capacity curves at a generator inlet of 190°F and a cooling-water inlet of 85°F, the cooling capacity factor is 1.13, the heat input factor 1.15 and the heat-medium flow corrections 1.0, so that, with a standard cooling capacity of 360 MBH,

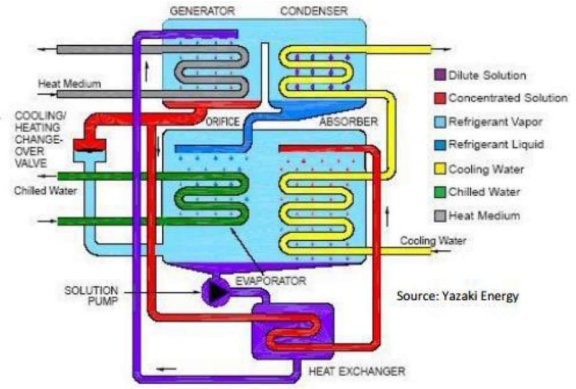

Fig. 11. Lithium bromide–water absorption cycle [1]. Source of the original diagram: Yazaki Energy.

$$Q_e = CCF \times HMFC \times Q_{e,std} = 1.13 \times 1.0 \times 360 = 406.8 \text{ MBH} \tag{38}$$

$$Q_g = HIF \times HMFC \times Q_{g,std} = 591.33 \text{ MBH} \tag{39}$$

$$COP = \frac{Q_e}{Q_g} = \frac{406.8}{591.33} \approx 0.69 \tag{40}$$

which is close to the rated COP of 0.68 in Table VI. The COP converts the monthly cooling load into an equivalent heating load on the collectors; because it is below one, each unit of cooling requires about 1.5 units of solar heat. The heat rejected to the cooling tower is 1100.46 MBH [1].

TABLE VI
Design Conditions of the Absorption Chiller-Heater (Model WFC-SH30) [1]

Parameter	Value
Heat medium inlet temperature	190°F
Heat medium flow	114.1 gpm
Cooling water inlet temperature	85°F
Cooling water flow	242.5 gpm
Chilled water outlet temperature	44.6°F
Chilled/hot water flow	72.6 gpm
Hot water outlet temperature	131°F
Coefficient of performance (COP)	0.68

 ©IJSRED: All Rights are Reserved

B. Assumptions and Thermal Loads

The school has 300 occupants, and the average daily DHW use is 5.7 L per person. The evacuated-tube collectors are tilted at the latitude plus 10°, 32.17° + 10° = 42.17°, which favors the low winter Sun and suits a system with a large heating load [1].

Designing assumptions and the equipment data are collected in Table VII. The monthly thermal loads are given in Table VIII: space heating dominates in January and cooling in July, while the DHW load is nearly constant. The loads total about 1.32×10^{12} J a year.

TABLE VII
DESIGN ASSUMPTIONS AND EQUIPMENT DATA [1]

Item	Value
Number of occupants	300
Average daily DHW use	5.7 L per person
Antifreeze	Propylene glycol, 50%
Average collector inlet fluid temperature	40°C
Storage tank capacity	180 gal
Collector tilt	42.17°
Heat exchanger effectiveness	0.92
Electric pump efficiency	0.88
Collector type	Evacuated tube
Collector gross area	4.287 m^2
Slope, F_RU_L	1.095 W/m^2·°C
Intercept, $F_R(\tau\alpha)$	0.509
Collector mass flow rate	0.0205 kg/s·m^2

TABLE VIII
MONTHLY THERMAL LOADS OF THE SCHOOL (10^{10} J) [1]

Month	DHW	Space heating	Cooling	Total
Jan	1.7	14.0	0	15.7
Feb	1.6	11.0	0	12.6
Mar	1.7	7.5	0	9.2
Apr	1.8	3.2	1.2	6.2
May	1.7	1.0	4.5	7.2
Jun	1.4	0	9.8	11.2
Jul	1.5	0	14.5	16.0
Aug	1.4	0	13.8	15.2
Sep	1.3	0	8.2	9.5
Oct	1.4	1.8	4.1	7.3
Nov	1.3	5.8	1.0	8.1
Dec	1.6	12.0	0	13.6
Year	18.4	56.3	57.1	131.8

C. Collector Efficiency, Number of Collectors and Solar Fraction

With a temperature difference of 10.36°F across the generator, the collector inlet temperature is 179.6°F. The collector (Sunda Seido 5-16) is rated with SRCC test data, in which category D ($T_i - T_a = 90$°F) represents the cooling season better than category E (144°F). In category D, under high radiation (2000 Btu/ft^2·day), the collector delivers 34,600 Btu per panel per day on a gross area of 46.15 ft^2, so its efficiency is

$$\eta_c = \frac{34\,600}{2000 \times 46.15} \approx 37.5\% \quad (41)$$

If the cooling load occurs over 6 h a day, the daily heat input is 591.33 MBH × 6 h = 3,547,980 Btu, and the number of collectors needed at the design condition is

$$N_c = \frac{3\,547\,980}{34\,600} \approx 103 \quad (42)$$

The utilizability method, with the slope of 1.095 W/m^2·°C, the intercept of 0.509 and a mean inlet temperature of 40°C, gives 181 collectors to meet the annual requirement for DHW, space heating and the heat that drives cooling [1]. The f-chart method then gives an annual solar fraction of 56%, with the monthly values of Fig. 12. The remaining thermal load is converted into an electrical load to be covered by the PV system (Table IX).

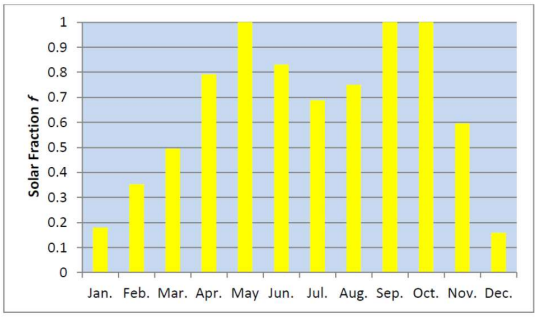

Fig. 12. Monthly solar fraction *f* from the f-chart calculation [1].

TABLE IX
HEAT LOAD MET BY SOLAR ENERGY AND LOAD REQUIRED FROM THE GRID [1]

Month	Heat load (10^{10} J)	Solar met (10^{10} J)	From grid (10^{10} J)	From grid (10^3 kWh)
Jan	15.7	9.8	5.9	16.4
Feb	12.6	9.6	3.0	8.3
Mar	9.2	7.4	1.8	5.0
Apr	6.2	5.3	0.9	2.5
May	7.2	6.1	1.1	3.1
Jun	11.2	9.7	1.5	4.2
Jul	16.0	12.5	3.5	9.7
Aug	15.2	12.2	3.0	8.3
Sep	9.5	7.9	1.6	4.4
Oct	7.3	5.9	1.4	3.9
Nov	8.1	5.8	2.3	6.4
Dec	13.6	8.9	4.7	13.1
Year	131.8	101.1	30.7	85.3

D. System Layout and Storage

The layout is shown in Fig. 13. The system comprises the 181 evacuated-tube collectors (ET), a single-stage LiBr–H_2O absorption chiller (ACH) with a COP of 0.68, an electric auxiliary heater (AH), a hot tank on the collector side (TK1) and a cold tank on the chiller side (TK2), pumps, valves, two heat exchangers (HE1, HE2), a cooling tower (CT), and the pipes, mixers, diverters and controllers that drive the working fluids through the cycle [1]. The DHW storage, which also serves space heating, was studied in TRNSYS with different preheat and main tank sizes (Table X). The larger preheat tank gave the highest annual solar fraction, 62.45%, and moving the

 ©IJSRED: All Rights are Reserved

auxiliary heating element from the top to the bottom of the tank raised it slightly, to 62.74%, so the bottom location was selected. The simulation output is shown in Fig. 14.

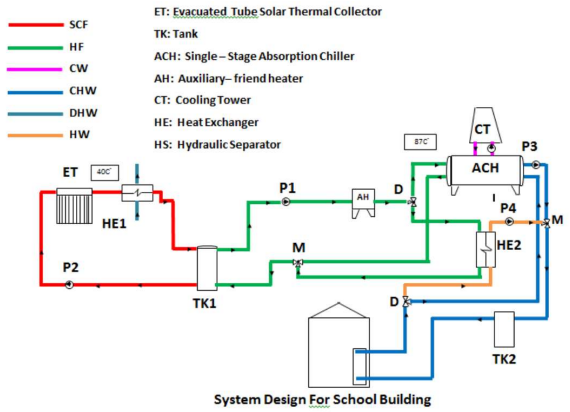

Fig. 13. Layout of the solar thermal system for the school building [1].

TABLE X
TRNSYS STORAGE SIMULATIONS: ANNUAL SOLAR FRACTION [1]

Case	Preheat tank	Main tank	Auxiliary element	Solar fraction
1	120	60	Top	62.45%
2	60	120	Top	57.64%
3	90	90	Top	58.94%
4	120	60	Bottom	62.74%

Tank sizes as reported in [1], where their unit is not stated.

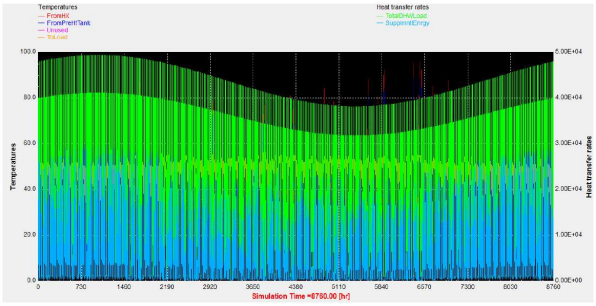

Fig. 14. TRNSYS simulation output for the DHW storage system over one year [1].

VI. PHOTOVOLTAIC SYSTEM DESIGN

The PV system is grid-connected and uses monocrystalline silicon modules rated at standard test conditions of 1000 W/m^2 and a cell temperature of 25°C (Table XI). The electrical load combines the electric heating carried over from the thermal system (about 3.0×10^4 kWh a year), the ordinary electrical load (about 1.90×10^5 kWh) and a small heat-pump allowance (600 kWh), about 2.2×10^5 kWh in total (Table XII). The array is rated at 228 kW DC and mounted on the roof at a 32° tilt facing due south. With a DC-to-AC derate factor of 0.77 the AC rating is

$$P_{AC} = 0.77 \times 228 = 175.56 \text{ kW} \quad (43)$$

and the number of modules follows from the array rating and the module capacity:

$$N_{PV} = \frac{P_{DC}}{P_{module}} = \frac{228 \text{ kW}}{0.395 \text{ kW}} \approx 578 \quad (44)$$

TABLE XI
PHOTOVOLTAIC MODULE AND SYSTEM SPECIFICATION [1]

Item	Value
Module	Grape Solar GS-S-395-Platinum, mono-Si
Rating, efficiency, area	395 W, 15.4%, 2.56 m^2
Number of modules	578
DC rating; derate factor	228 kW; 0.77
AC rating	175.56 kW
Array	Fixed roof mount, tilt 32°, azimuth 180°
Weather data	Gharyan (TMY, estimated)
Utility electricity cost	0.04 $/kWh
PV electricity cost	0.22 $/kWh

PVWatts gives an annual AC output of about 2.78×10^5 kWh [1]; the monthly values in Table XII sum to 2.89×10^5 kWh. From November to February the load exceeds the output and the school imports about 1.42×10^4 kWh, while from March to October the array exports a surplus of about 8.1×10^4 kWh, so the design is above net zero over the year. Table XII also lists the monthly output estimated in this paper with (36) for the same array at both sites; these estimates are discussed in Section VII.

TABLE XII
MONTHLY ELECTRICAL LOAD AND AC OUTPUT OF THE 228 kW ARRAY (MWh)

Month	Load [1]	PVWatts [1]		Estimate, (36)	
		AC output	Load − AC	Gharyan	Dayton
Jan	23.3	19.0	+4.3	27.1	17.5
Feb	20.1	15.5	+4.6	25.8	18.2
Mar	19.3	23.5	−4.2	30.4	22.5
Apr	18.0	26.5	−8.5	30.5	23.7
May	16.7	28.5	−11.8	32.6	25.8
Jun	15.8	30.5	−14.7	32.0	25.2
Jul	18.0	31.5	−13.5	34.5	25.5
Aug	17.8	30.0	−12.2	35.7	25.3
Sep	15.4	26.0	−10.6	33.3	23.6
Oct	17.3	23.0	−5.7	33.2	22.1
Nov	17.1	16.5	+0.6	29.8	16.1
Dec	22.7	18.0	+4.7	27.5	13.5
Year	221.5	288.5	−67.0	372.3	259.0

Load − AC: positive values are imports from the grid, negative values exports. Estimates for 32° tilt at Gharyan and 39.9° at Dayton.

VII. COMPARISON OF GHARYAN AND DAYTON

A. Solar Geometry

Table XIII applies (17), (18), (12) and (14) to the 21st day of each month at both latitudes. Gharyan's noon Sun stands 7.7° higher than Dayton's throughout the year: 34.4° against 26.7° at the December solstice and 81.3° against 73.5° in June. The December noon air mass is 1.77 against 2.23, and the clear-sky direct intensity 0.80 against 0.73 kW/m^2. Dayton's days are about 0.7 h longer in June and 0.7 h shorter in December. For an array tilted at the local latitude the noon incidence angle equals |δ| at both sites, so the latitude-tilt rule transfers directly;

 ©IJSRED: All Rights are Reserved

what differs between the sites is the amount of light that reaches the array.

TABLE XIII
CALCULATED NOON SOLAR GEOMETRY AND CLEAR-SKY DIRECT INTENSITY ON THE 21ST DAY OF EACH MONTH, GHARYAN (G, 32.17° N) AND DAYTON (D, 39.90° N)

Month	δ (°)	Noon β (°)		Air mass		I_D (kW/m²)		Day length (h)	
		G	D	G	D	G	D	G	D
Jan	−20.1	37.7	30.0	1.64	2.00	0.82	0.76	10.2	9.6
Feb	−11.2	46.6	38.9	1.38	1.59	0.87	0.83	11.0	10.7
Mar	−0.4	57.4	49.7	1.19	1.31	0.91	0.88	12.0	12.0
Apr	11.6	69.4	61.7	1.07	1.14	0.93	0.92	13.0	13.3
May	20.1	78.0	70.2	1.02	1.06	0.94	0.93	13.8	14.4
Jun	23.4	81.3	73.5	1.01	1.04	0.94	0.94	14.1	14.8
Jul	20.4	78.3	70.5	1.02	1.06	0.94	0.93	13.8	14.4
Aug	11.8	69.6	61.9	1.07	1.13	0.93	0.92	13.0	13.3
Sep	−0.2	57.6	49.9	1.18	1.31	0.91	0.88	12.0	12.0
Oct	−11.8	46.1	38.3	1.39	1.61	0.87	0.83	11.0	10.7
Nov	−20.4	37.4	29.7	1.65	2.02	0.82	0.76	10.2	9.6
Dec	−23.4	34.4	26.7	1.77	2.23	0.80	0.73	9.9	9.2

B. Solar Resource

Fig. 15 and Table V compare the two climates. Gharyan receives 2129 kWh/m² a year on a horizontal surface against 1438 kWh/m² at Dayton, 48% more, and about twice as much in November and December (3.3 against 1.5 kWh/m² per day in December). Geometry explains only part of the difference. From (33), the December extraterrestrial radiation is 5.16 kWh/m² per day at Gharyan and 3.84 at Dayton, a ratio of 1.34, whereas the clearness index is 0.64 against 0.39, a ratio of 1.64. In June the extraterrestrial values are almost equal (11.5 and 11.6 kWh/m²), because Dayton's longer day offsets its lower Sun, and the whole difference comes from the clearer sky ($\bar{K}_T$ = 0.71 against 0.53). Over the year the clearness index is 0.68 at Gharyan and 0.50 at Dayton. On the plane of the arrays, (35) gives 2337 kWh/m² a year for Gharyan at 32° and 1570 kWh/m² for Dayton at 39.9°, against 1604 kWh/m² in the NREL tilt data (Fig. 10). Gharyan's December irradiation on the tilted plane, 5.3 kWh/m² per day, is more than twice Dayton's 2.5 kWh/m².

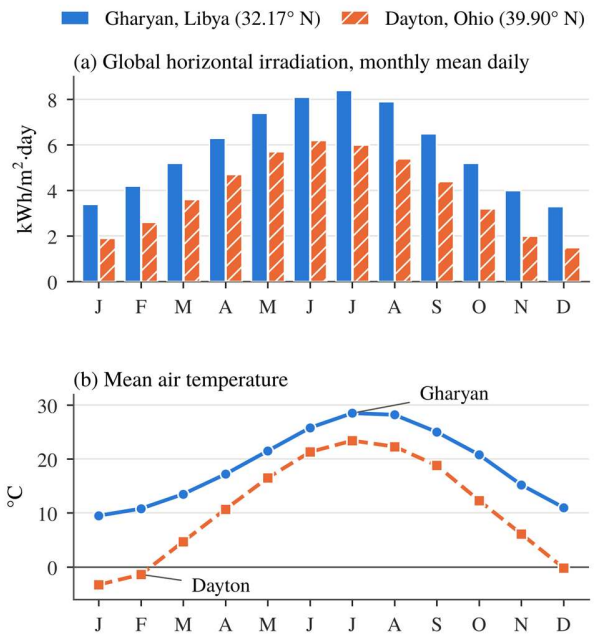

Fig. 15. Monthly climate of Gharyan [1] and Dayton [24]: (a) mean daily global horizontal irradiation; (b) mean air temperature.

C. Heating and Cooling Demand

The climates load a combi-system in opposite ways (Fig. 16). Dayton has 3171 heating and 492 cooling degree-days a year, Gharyan 1030 and 1210. Dayton's thermal demand is therefore dominated by space heating in the months with the least sunshine, when its clearness index is only 0.39–0.45, so a solar heating system there delivers its smallest fraction in mid-winter. In Gharyan the largest thermal load is cooling, and it coincides with the highest radiation (Table VIII and Table V); this match is the main argument for solar absorption cooling in Libya. A collector field sized for Dayton's winter is therefore not automatically right for Gharyan: the winter heating load needs less collector area, while the summer generator demand, at a COP of 0.68, needs more.

 ©IJSRED: All Rights are Reserved

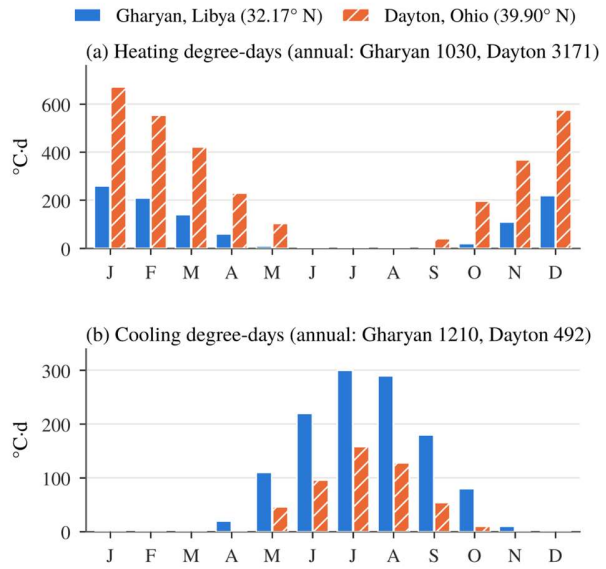

Fig. 16. Monthly degree-days at Gharyan [1] and Dayton [24]: (a) heating; (b) cooling.

D. Photovoltaic Yield

Fig. 17 and Table XII compare the monthly output of the same 228 kW array estimated with (36) and (37). Gharyan gives about 3.72×10^5 kWh a year, a specific yield of 1630 kWh/kWp, and Dayton 2.59×10^5 kWh, or 1140 kWh/kWp (1160 kWh/kWp with the NREL tilt data). Higher cell temperatures cost Gharyan about 9% of its output against 6% at Dayton, but the irradiation advantage dominates. The estimated output exceeds the Gharyan load in every month, so on a monthly basis the school would export about 1.5×10^5 kWh a year, and about 135 kW, or some 340 modules of 395 W, would meet the annual load: 41% fewer modules than in the design. The output reported for Gharyan in [1] corresponds to 1220 kWh/kWp, within 5–7% of the Dayton estimate and 25% below the Gharyan estimate. That PVWatts run used an estimated weather file (Table XI), and it should be repeated with a measured or satellite-derived file for Gharyan.

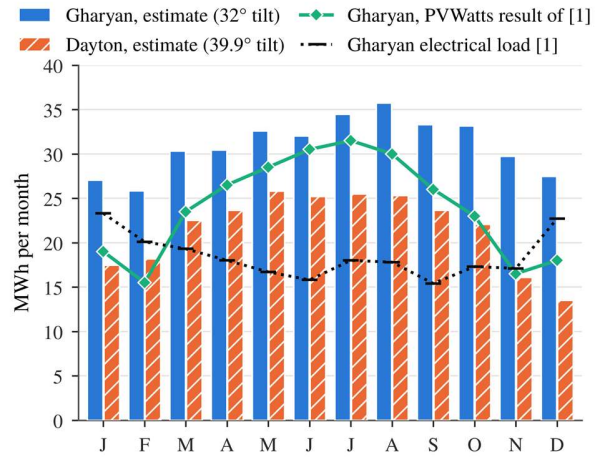

Fig. 17. Monthly AC output of the 228 kW array estimated with (36) for Gharyan and Dayton, compared with the PVWatts result and the electrical load of [1].

E. Economics and Emissions

The economic comparison is decided by tariffs. In 2024 the average retail price of electricity in Ohio was 11.29 US cents/kWh, and the state's generation emitted 1005 lb of CO_2 per MWh, or 0.456 kg/kWh [30]. In Libya the tariff is LYD 0.04 per kWh, about US$0.005–0.008 and among the lowest in the world, and electricity generation consumed 10 billion m^3 of natural gas and 5 million barrels of crude oil in 2023 [31]. At these prices the estimated Dayton output is worth about US$29,000 a year to the school, but the larger Gharyan output only about US$1,900–3,000. This is why the payback of about five years reported for the Dayton school [1] cannot be expected in Gharyan, where the case for the system rests on reliability during outages and on the fuel and subsidy costs borne by the state, rather than on the school's bill. The emission savings, by contrast, are larger in Gharyan. With the combined-margin factor of 0.632 kg CO_2/kWh for intermittent generation in Libya [32], the estimated Gharyan output would avoid about 235 t of CO_2 a year (176 t on the PVWatts output of [1]), whereas at Ohio's average emission rate the Dayton array would avoid about 118 t; the two factors are defined differently, so the comparison is indicative.

F. What Transfers and What Does Not

Table XIV summarizes the comparison. The design methods and the latitude-tilt rule transfer from Dayton to Gharyan. The collector and module counts, the monthly solar fractions and the PV output do not, because they depend on the local balance of heating and cooling, on cloudiness and on temperature. The Gharyan design of [1] nevertheless uses the same numbers as the Dayton design: 181 collectors, 578 modules and a 56% solar fraction. Its monthly solar fractions (Fig. 12), below 0.2 in December and January, are typical of a heating-dominated climate and conflict with the 62% of the January load met by solar heat in Table IX. The radiation spreadsheet of [1] helps to explain the coincidence: it uses the Gharyan latitude, but its monthly horizontal irradiation (1.63–6.22 kWh/m^2 per day, annual mean 4.0) and air temperatures (−0.5 to 24.3°C, annual mean 12.4°C) are close to the Dayton data of Table V (3.9 kWh/m^2 per day and 10.9°C) and far from the Gharyan data (5.8 kWh/m^2 per day and 18.9°C). The thermal and PV results should therefore be recomputed from the Gharyan data before the design is built.

 ©IJSRED: All Rights are Reserved

TABLE XIV
SUMMARY OF THE SITE AND DESIGN COMPARISON

Quantity	Gharyan, Libya	Dayton, Ohio
Latitude, longitude	32.17° N, 13.02° E	39.90° N, 84.22° W
Elevation	≈550 m	306 m
Mean annual temperature	18.9°C	10.9°C
Coldest/warmest month	9.5/28.5°C	−3.3/23.4°C
Heating/cooling degree-days	1030/1210 °C·d	3171/492 °C·d
Global horizontal irradiation	2129 kWh/m^2	1438 kWh/m^2
Annual clearness index	0.68	0.50
Irradiation at latitude tilt	2337 kWh/m^2	1570 kWh/m^2
Noon altitude, Dec/Jun	34.4°/81.3°	26.7°/73.5°
Day length, Dec/Jun	9.9/14.1 h	9.2/14.8 h
PV specific yield (estimate)	1630 kWh/kWp	1140 kWh/kWp
AC output of 228 kW array	372 MWh	259 MWh
Collectors/modules [1]	181/578	181/578
Annual solar fraction [1]	56%	>56%
Electricity price	LYD 0.04/kWh [31]	11.29 US¢/kWh [30]
Grid emission factor	0.632 kg/kWh [32]	0.456 kg/kWh [30]
Avoided CO_2 (estimate)	≈235 t/year	≈118 t/year
Simple payback [1]	None at current tariff	≈5 years

VIII. DISCUSSION AND LIMITATIONS

The methods used are established. The f-chart and phi-f chart methods remain accepted tools for preliminary design [21], PVWatts is a standard estimator of PV output [29], and crystalline silicon is a conservative choice of module. Several values in [1] do not yet agree with one another and should be reconciled before the design is used. The annual requirement used with the utilizability method is 1.80×10^{12} J, whereas the loads in Table VIII total 1.32×10^{12} J. The solar heat in Table IX meets 77% of the load, whereas the f-chart solar fraction is 56%. The stated annual PV output, 2.78×10^5 kWh, is less than the sum of the monthly values, 2.89×10^5 kWh, and other stated totals of [1] differ slightly from the sums of the monthly values reported here. The heat drawn from the grid in Table IX, 8.5×10^4 kWh, is 2.8 times the electric heating load of 3.0×10^4 kWh carried into the PV design, a ratio that would correspond to a heat pump but is not explained. The latitude is entered as 31.13° in one place and 32.17° in another, the unit of the tank sizes in Table X is not stated, and the 180-gal (0.68 m^3) tank of Table VII amounts to less than 1 L per m^2 of the 776 m^2 collector area, far outside the 37.5–300 L/m^2 range of the f-chart storage correction. The solar constant should be updated from 1.353 to about 1.361 kW/m^2 [22], although this changes no result materially.

The economics also need further work. With a utility price of 0.04 $/kWh and a PV electricity cost of 0.22 $/kWh (Table XI), PV electricity costs more than five times as much as the grid power it replaces. The IMF gives the Libyan tariff as LYD 0.04 per kWh [31], which suggests that the utility price in [1] is in dinars and that the gap is wider still. Two points soften this result. The PV cost is dated: utility-scale PV averaged 0.044 $/kWh in 2025, 89% less than in 2010 [16], and although a rooftop system costs more than a utility plant, a current local quotation would probably be far below 0.22 $/kWh. In addition, the school's problem is reliability as much as price, and the value of lessons not lost to outages does not appear in a tariff comparison.

Three items are outside the present design. A grid-connected system without batteries shuts down during an outage, so battery storage or a hybrid inverter sized for the critical loads is needed if the system is to keep the school running; storage costs differ widely among technologies and deserve their own analysis [11]. Dust reduces PV output in dry regions, so a cleaning schedule should be part of the design [19]. The avoided emissions estimated in Section VII rest on a default grid factor and should be refined with Libyan generation data; with energy payback times of 1.7–2.7 years for monocrystalline systems [14] the array would also repay its manufacturing energy early in its life. Finally, the comparison relies on 1961–1990 averages for Dayton, estimated data for Gharyan and a monthly PV model. An hourly simulation with satellite-derived typical years for both sites would refine the numbers, but it is unlikely to change the conclusions, because the differences in irradiation and tariff are much larger than the uncertainty of the model.

IX. CONCLUSION

This paper has combined a review of solar technologies, the physics of solar radiation and Sun–Earth geometry, and the design of a net-zero energy solar system for an elementary school in Gharyan, Libya, and has compared the site with Dayton, Ohio, where the main precedent for the design was developed. Crystalline silicon PV is mature and cheap, and the remaining problems are storage, high temperature, dust and integration with thermal systems and the grid. A south-facing array tilted near the latitude receives the noon Sun within 23.45° of its normal in every season at both sites. The design of [1] combines 181 evacuated-tube collectors and a LiBr–H_2O chiller of COP 0.68, for an annual solar fraction of 56%, with a 228 kW array of 578 modules whose reported output of 2.78×10^5 kWh exceeds the load of about 2.2×10^5 kWh; storage simulations give a best DHW solar fraction of 62.74% with the auxiliary element at the bottom of the tank.

The comparison shows that Gharyan receives 48% more global irradiation than Dayton, has one third of its heating degree-days and 2.5 times its cooling degree-days, and would produce about 44% more electricity from the same array, so that about 135 kW would meet the Gharyan load. The design methods transfer between the two sites; the collector numbers, solar fractions and PV output do not. Because the Libyan tariff is below 1 US cent/kWh against 11.3 cents in Ohio, the case for the system in Libya rests on reliability and on the state's fuel and subsidy costs rather than on the school's bill. Future work should recompute the thermal and PV design from a single consistent set of Gharyan data, add battery storage for operation during outages, update the costs with local quotations, and refine the avoided emissions, estimated here at about 235 t of CO_2 a year, with Libyan grid data.

REFERENCES

[1] H. Mohamed et al., "Designing solar energy systems with the integration of net zero energy building technology," *Sciences and Technologies.*, vol. 8, no. 2, pp. 68–80, 2024.

 ©IJSRED: All Rights are Reserved

[2] I. Sartori, A. Napolitano, and K. Voss, "Net zero energy buildings: A consistent definition framework," *Energy Build.*, vol. 48, pp. 220–232, 2012, doi: 10.1016/j.enbuild.2012.01.032.

[3] A. J. Marszal *et al.*, "Zero energy building – A review of definitions and calculation methodologies," *Energy Build.*, vol. 43, no. 4, pp. 971–979, 2011, doi: 10.1016/j.enbuild.2010.12.022.

[4] C. B. Honsberg and S. G. Bowden, "Photovoltaics education website," 2019. [Online]. Available: https://www.pveducation.org

[5] M. A. Green, "Photovoltaic principles," *Physica E*, vol. 14, no. 1–2, pp. 11–17, 2002, doi: 10.1016/S1386-9477(02)00354-5.

[6] D. M. Chapin, C. S. Fuller, and G. L. Pearson, "A new silicon p-n junction photocell for converting solar radiation into electrical power," *J. Appl. Phys.*, vol. 25, no. 5, pp. 676–677, May 1954, doi: 10.1063/1.1721711.

[7] J. Zhao, A. Wang, M. A. Green, and F. Ferrazza, "19.8% efficient 'honeycomb' textured multicrystalline and 24.4% monocrystalline silicon solar cells," *Appl. Phys. Lett.*, vol. 73, no. 14, pp. 1991–1993, Oct. 1998, doi: 10.1063/1.122345.

[8] W. Shockley and H. J. Queisser, "Detailed balance limit of efficiency of p-n junction solar cells," *J. Appl. Phys.*, vol. 32, no. 3, pp. 510–519, Mar. 1961, doi: 10.1063/1.1736034.

[9] J. Pastuszak and P. Węgierek, "Photovoltaic cell generations and current research directions for their development," *Materials*, vol. 15, no. 16, Art. no. 5542, Aug. 2022, doi: 10.3390/ma15165542.

[10] M. Grätzel, "Solar energy conversion by dye-sensitized photovoltaic cells," *Inorg. Chem.*, vol. 44, no. 20, pp. 6841–6851, Oct. 2005, doi: 10.1021/ic0508371.

[11] B. Zakeri and S. Syri, "Electrical energy storage systems: A comparative life cycle cost analysis," *Renew. Sustain. Energy Rev.*, vol. 42, pp. 569–596, 2015, doi: 10.1016/j.rser.2014.10.011.

[12] W. Jing, C. H. Lai, W. S. H. Wong, and M. L. D. Wong, "Battery-supercapacitor hybrid energy storage system in standalone DC microgrids: A review," *IET Renew. Power Gener.*, vol. 11, no. 4, pp. 461–469, Mar. 2017, doi: 10.1049/iet-rpg.2016.0500.

[13] Z. Wang *et al.*, "Hybrid solar energy device for simultaneous electric power generation and molecular solar thermal energy storage," *Joule*, vol. 8, no. 9, pp. 2607–2622, 2024, doi: 10.1016/j.joule.2024.06.012.

[14] J. Peng, L. Lu, and H. Yang, "Review on life cycle assessment of energy payback and greenhouse gas emission of solar photovoltaic systems," *Renew. Sustain. Energy Rev.*, vol. 19, pp. 255–274, 2013, doi: 10.1016/j.rser.2012.11.035.

[15] R. R. Hernandez *et al.*, "Environmental impacts of utility-scale solar energy," *Renew. Sustain. Energy Rev.*, vol. 29, pp. 766–779, 2014, doi: 10.1016/j.rser.2013.08.041.

[16] International Renewable Energy Agency, *Renewable Power Generation Costs in 2025*. Abu Dhabi, UAE: IRENA, 2026. [Online]. Available: https://www.irena.org/Publications/2026/Jul/Renewable-Power-Generation-Costs-in-2025

[17] N. Kannan and D. Vakeesan, "Solar energy for future world: A review," *Renew. Sustain. Energy Rev.*, vol. 62, pp. 1092–1105, 2016, doi: 10.1016/j.rser.2016.05.022.

[18] E. Kabir, P. Kumar, S. Kumar, A. A. Adelodun, and K.-H. Kim, "Solar energy: Potential and future prospects," *Renew. Sustain. Energy Rev.*, vol. 82, pp. 894–900, Feb. 2018, doi: 10.1016/j.rser.2017.09.094.

[19] M. Mani and R. Pillai, "Impact of dust on solar photovoltaic (PV) performance: Research status, challenges and recommendations," *Renew. Sustain. Energy Rev.*, vol. 14, no. 9, pp. 3124–3131, Dec. 2010, doi: 10.1016/j.rser.2010.07.065.

[20] A. Mellit and S. A. Kalogirou, "Artificial intelligence techniques for photovoltaic applications: A review," *Prog. Energy Combust. Sci.*, vol. 34, no. 5, pp. 574–632, 2008, doi: 10.1016/j.pecs.2008.01.001.

[21] J. A. Duffie and W. A. Beckman, *Solar Engineering of Thermal Processes*, 4th ed. Hoboken, NJ, USA: Wiley, 2013.

[22] G. Kopp and J. L. Lean, "A new, lower value of total solar irradiance: Evidence and climate significance," *Geophys. Res. Lett.*, vol. 38, no. 1, Art. no. L01706, Jan. 2011, doi: 10.1029/2010GL045777.

[23] F. Kasten and A. T. Young, "Revised optical air mass tables and approximation formula," *Appl. Opt.*, vol. 28, no. 22, pp. 4735–4738, Nov. 1989, doi: 10.1364/AO.28.004735.

[24] W. Marion and S. Wilcox, "Solar radiation data manual for flat-plate and concentrating collectors," Nat. Renew. Energy Lab., Golden, CO, USA, Tech. Rep. NREL/TP-463-5607, Apr. 1994.

[25] S. A. Klein, W. A. Beckman, and J. A. Duffie, "A design procedure for solar heating systems," *Sol. Energy*, vol. 18, no. 2, pp. 113–127, 1976.

[26] S. A. Klein and W. A. Beckman, "A general design method for closed-loop solar energy systems," *Sol. Energy*, vol. 22, no. 3, pp. 269–282, 1979.

[27] D. G. Erbs, S. A. Klein, and J. A. Duffie, "Estimation of the diffuse radiation fraction for hourly, daily and monthly-average global radiation," *Sol. Energy*, vol. 28, no. 4, pp. 293–302, 1982.

[28] S. A. Klein, "Calculation of monthly average insolation on tilted surfaces," *Sol. Energy*, vol. 19, no. 4, pp. 325–329, 1977.

[29] A. P. Dobos, "PVWatts version 5 manual," Nat. Renew. Energy Lab., Golden, CO, USA, Tech. Rep. NREL/TP-6A20-62641, 2014. [Online]. Available: https://www.osti.gov/biblio/1158421

[30] U.S. Energy Information Administration, "Ohio electricity profile 2024," 2025. [Online]. Available: https://www.eia.gov/electricity/state/ohio/ (accessed Oct. 19, 2026).

[31] International Monetary Fund, "Libya: Selected issues," IMF Country Rep. No. 25/149, Washington, DC, USA, Jun. 2025.

[32] IFI Technical Working Group on GHG Accounting, "The IFI dataset of default grid factors," ver. 2.0, Jul. 2019. [Online]. Available: https://unfccc.int/sites/default/files/resource/Harmonized_Grid_Emission_factor_data_set.pdf (accessed Oct. 20, 2026).

 ©IJSRED: All Rights are Reserved